Journal of Applied Fluid Mechanics, Vol. 18, No. 4, pp. 992-1006, 2025.
Available online at www.jafmonline.net, ISSN 1735-3572, EISSN 1735-3645.
https://doi.org/10.47176/jafm.18.4.2922

Experimental Investigations of Self-adjusting Bionic Flaps on Low-aspect Ratio Wings

A. Verma[1†], V. Kulkarni[1] and S. Shinde[2]

[1] *Department of Mechanical Engineering, Indian Institute of Technology Guwahati, Guwahati, Assam, 781039, India*
[2] *Department of Mechanical Engineering, Indian Institute of Technology Kanpur, Kanpur, U.P., 208016, India*

†*Corresponding Author Email: anand2016@iitg.ac.in*

ABSTRACT

Self-adjusting flexible flap is a biomimetic passive flow control device, which is evolved by emulating the covert feathers on the upper wing of a bird. The effectiveness of such a flap was explored mostly for infinite or high aspect ratio (*AR*) wings from low to high Reynolds numbers (*Re*) in prior studies. However, the aerodynamic characteristics of a high *AR* wing are completely different from the lower one due to wingtip vortices. Therefore, in the present work, this flap is tested on a S5010 profiled wing of two different low *AR*s, 2.0 and 1.0, in the *Re* range of MAVs application. Three flap chord lengths (0.12*c*, 0.15*c*, and 0.20*c*) are examined at various chord-wise positions (0.3*c* to 0.8*c*). Results show that the optimal performance enhancement is achieved when flaps cover 80% of the wingspan for *AR* 2.0 and 70% for *AR* 1.0. The flap does not impact pre-stall wing performance, but it significantly improves post-stall lift and drag characteristics over the clean wing. Increasing the flap chord from 0.12*c* to 0.15*c* increases wing performance, but increases beyond 0.15*c* provide no additional beneficial effects. The optimal chord-wise position of the flap for better performance enhancement is near the mid-chord for both models. Multiple flap configurations have a relatively lower lift-enhancing capability than single flap configurations. The effect of *Re* on the flap effectiveness decreases with decreasing *AR* of the wing.

Article History

Received June 16, 2024
Revised September 6, 2024
Accepted October 20, 2024
Available online February 4, 2025

Keywords:

Wind tunnel testing
Low aspect ratio
S5010 profiled wing
Aerodynamic coefficients
Bio-inspired
Self-adjustable flap

1. INTRODUCTION

Micro air vehicles (MAVs) are a special form of unmanned aircraft which are evolving rapidly every year due to their vast applications in civil and military sectors. Apart from these, such vehicles are designed to serve various operations like surveillance missions, border patrolling, disaster relief services, and improving communications in urban areas. The main advantage of such vehicles is their small size, which allows them to be conveyed by a single operator, difficulty in sighting, and ease of operation as well as maintenance. For the efficient design and development of MAVs, various factors must be taken into account, viz. aerodynamics, maneuverability, propulsion system, power unit, and various accessories (cameras, sensors, etc.) (Mueller et al., 2007). Among these, the major area of serious concern is the aerodynamic efficiency of the wing because such vehicles have limited wing dimensions and power input, due to which they operate under a low Reynolds number (*Re*) range. In general, their operational *Re* range is 1×10^4 to 1×10^5 (Mueller, 1999). Prior studies suggested that the *Re* has a substantial influence on the aerodynamic performance of conventional airfoils (McMasters & Henderson, 1979; Mueller, 1999). Even though conventional airfoils have been proven to have the best aerodynamic characteristics at *Re* above 1×10^6, their performance in terms of maximum lift coefficients and lift-over-drag ratio degrades drastically when *Re* falls below 1×10^5 due to excessive flow separation (McMasters & Henderson, 1979). Typically, flow separation over an airfoil is directly associated with loss of lift, increased pressure drag, and generation of aerodynamic noise (Gerakopulos et al., 2010; Winslow et al., 2018; Park et al., 2020). Therefore, controlling flow separation becomes very important for the effective design of such low-speed vehicles.

Aerodynamicists all over the globe are contributing to addressing these issues through modifications in the wing configuration or by adopting flow control approaches. The flow control techniques are broadly categorized into active and passive strategies (Gad-el-Hak & Pollard, 1998). Synthetic jets, blowing, suction, plasma actuators, etc., are

NOMENCLATURE

A	wing surface area	D	drag force
AR	aspect ratio	L	lift force
AoA	angle of attack	M	pitching moment
b	wingspan	MAV	Micro Air Vehicle
c	wing chord	Re	Reynolds number
c_f	flap chord	S	flap span
C_D	drag coefficient	U_∞	freestream velocity
C_L	lift coefficient	ρ	air density
C_{Lmax}	maximum lift coefficient	υ	kinematic viscosity of air
$C_{M,0.25c}$	pitching moment coefficient about quarter-chord		

some active techniques that were used to improve the aerodynamic performance of the airfoil/wing (Kim et al., 2007; Rizzetta & Visbal, 2008, 2012; Baljit et al., 2017). Additionally, several passive techniques were also employed to enhance the performance of airfoils or wings, including the implementation of a gurney flap, self-actuating flap, creation of a cavity on the suction surface, etc. (Meyer et al., 2007; Cravero, 2017; Lam & Leung, 2018; Verma & Kulkarni, 2021). The active approaches require a power unit to operate, while the passive ones require no power source. Consequently, the implementation of an active strategy in small-scale aircraft creates difficulty for the designer due to constraints of wing size, power unit, and weight. Therefore, the current study explores the self-actuating flap as a passive flow separation control approach. This method is completely inspired by a bird's flight. Because of their morphological system, birds can fly at incredibly low speeds and with extremely high angles of attack (*AoA*) (Bechert et al., 1997; Azuma, 1992). This potential not only helps them to execute their preferred trajectories with effortlessness, but it also lets them land softly in congested places and take off quickly from the small nest. In addition, birds have the ability to naturally deal with flow separation using the upper wing surface of the covert feathers. An example of this is shown in Fig. 1. It has been noticed that the wing coverts tend to pop-up naturally during their landing approach *AoA* or in other situations, such as flight at high *AoA* or while passing through gusty wind situations. In contrast, the same coverts are then instantly returned to their usual location by reducing the wing's *AoA*. This type of wing action is retained sinusoidally during low-speed flying.

Fig. 1 A Bar-headed goose's wing with deflection of covert feathers to prevent the propagation of flow separation (*Captured by the first author*)

These passive pop-up covert feathers are theorized to control flow separation and allow higher lift at low speeds, as well as to improve the bird's flight performance at high *AoA*. Liebe explained the behavior of a bird's feather as a biological high-lift device and suggested that it acts as a brake to prevent the propagation of the separation bubble towards the leading edge (Bechert et al., 1997). On Liebe's suggestions, this concept was initially tested in flight experiments on the fighter aircraft Messerschmitt Me-109 in early 1938. In this experiment, a thin leather sheet (known as self-adjustable flap / self-movable flap / lift enhancing effectors) was placed spanwise on the upper surface of the aircraft's wing to imitate a bird's covert feathers function. The results showed that the flying behavior of the aircraft with this attachment was satisfactory at a low *AoA*. However, when flying at a higher *AoA*, it was difficult to handle the aircraft, primarily due to the aerodynamic asymmetry of the wing. Much later in this event, various experimental investigations were conducted by putting lightweight, thin sheets on the upper surface of the wing to replicate the motion of the bird's wing coverts (Bramesfeld & Maughmer, 2002; Schatz et al., 2004; Kernstine et al., 2008; Wang & Schlüter, 2012; Arivoli & Singh, 2016; Hao et al., 2022). Those studies concluded a satisfactory effect of this self-movable passive flap on the performance of the airfoil/wing for post-stall *AoA* at low to high *Re*. Initially, the flap remains attached to the surface of the wing, but when the flow begins to separate, the flap gradually rises due to the momentum of reverse flow and continuously adjusts itself to an equilibrium position that obstructs the progression of the separation bubble. These lift-enhancing effectors act as pressure dams that reduce the adverse pressure effect of separation on the pressure distribution of attached flow upstream of the flap location, resulting in

lower pressure upstream of the upper surface than downstream of the flap (Bramesfeld & Maughmer, 2002).

Bechert et al. (1997) explored how these effectors functioned and proved the feasibility of thin flaps as lift enhancement effectors in the high *Re* range of 1×10^6 to 2×10^6. Similarly, Meyer et al. (2007) found an improvement in the lift at higher *AoA* for a wing section using passive flaps closer to the trailing edge for the same *Re*. Further, this study was extended to a low *Re* regime to examine the flap effectiveness up to $Re = 3 \times 10^4$ - 4×10^4 (Schlüter, 2010). Moreover, the aerodynamic characteristics of the wing resulting from installing the flap depend on various factors such as flap size and its material (weight, stiffness, and flexibility), installation location on the wing surface, and hinge configuration for its easy rotation. Kernstine et al. (2008) explored the flap material selection and suggested that the flap should be made of a material that is thin, lightweight, flexible, and should have adequate strength to prevent tearing. These properties allow the flap to follow the curvature of the airfoil, which avoids loss of lift at low *AoA* and prevents tearing against aerodynamic forces at high *AoA*. Other parameters that influence flap performance are flap width, hinge arrangement, and its location on the wing surface. Most of the earlier studies accounted for flap widths between 10% and 40% of the chord length and found a favorable effect on the lift of the airfoil in the post-stall region (Meyer et al., 2007; Kernstine et al., 2008; Schlüter, 2010; Wang & Schlüter, 2012). The flap size below 10% of the chord was found to be inadequate to obstruct the reverse flow during the stall. While flap lengths, more than 40% of the chord demonstrated lift loss at lower angles of attack due to premature flap deployment caused by a reduction in surface pressure across the flap. Further, any flap position was not found universally effective for all flap lengths and wing sections, but it was noted to be dependent on the pressure distribution and boundary layer separation characteristics of the wing surface (Meyer et al., 2007; Altman & Allemand, 2016). For example, Arivoli et al. noticed a considerable lift enhancement for the rectangular flat plate planform when the flap was placed close to the trailing edge (0.8*x/c*) (Arivoli & Singh, 2016; Arivoli et al., 2020). In the case of the Zimmerman planform, the flapping effect was more significant when it was fixed at the maximum span location (0.4 *x/c*) of the wing for the same flap length and flow conditions. It was revealed that, for a wing with leading edge stall behavior, placing the flap near the trailing edge may not be useful since the reverse flow has already spread on the wing surface before reaching the trailing edge of the flap. Similarly, a flap does not create a favorable effect for a wing with trailing edge stall characteristics when it is positioned in an upstream location on the wing.

1.1 Research Gap

Previous studies have demonstrated that self-deployed flaps are a feasible technique for improving the lift and stall characteristics of an infinite wing or airfoil under various *Re* regimes. Most investigations have focused on the effect of parametric variation in flaps on the performance of conventional airfoils or large *AR* wings. However, there is a lack of information and understanding available regarding the application of this passive flap in low *AR* wings. In fact, the aerodynamic characteristics of a low *AR* wing are entirely different from those of a similar wing with a high *AR* or its airfoil section (Mizoguchi & Itoh, 2013; Karasu et al., 2018). This is mainly caused by wingtip vortices, which induce downwash on the upper wing surface. As an effect of this downwash, pressure distribution over the surface changes, consequently affecting the performance of the wing. Further, as the wing *AR* reduces, the wingtip vortices become more significant. Hence, it is interesting to explore flap effectiveness for low *AR* wings, which would be beneficial for fixed-wing MAV applications. Although Altman & Allemand (2016) investigated the influence of flap on the finite wing's performance, but the studies were unable to predict flap effectiveness based on an *AR* below 3.0. As it was reported that the performance of the wing was found to be relatively similar to *AR* of 3.0 and above, whereas, for *AR* below 3.0, a significant effect of *AR* on the wing characteristics was observed (Mizoguchi & Itoh, 2013). As a result, the preceding investigation is insufficient to quantify the effectiveness of passive flaps for the wings with an *AR* below 3.0.

1.2 Present Objective

In view of the abovementioned research gap, the present studies are planned to explore the impact of self-actuating flaps on the performance of wings with *AR*s below 2.0, specifically within the *Re* range relevant to MAVs. The primary objective commences with a detailed investigation into flap dynamics, concentrating on the analysis of parametric variations in flap span lengths to determine the optimal span size for enhanced performance. Building upon this foundation, the subsequent phase of our exploration shifts focus to examine the effects of varying flap chord lengths and their chord-wise placement on the wing surface. Through this systematic exploration, our overarching goal is to contribute valuable findings that directly address key parameters crucial for optimizing the flying characteristics of MAVs, ultimately improving their efficiency and maneuverability. The details of the wing models, experimental setup, and aerodynamic measurements are explained in the following sections.

2. EXPERIMENTAL SETUP

Present investigations are carried out in an open circuit subsonic wind tunnel located at the Department of Mechanical Engineering, Indian Institute of Technology, Guwahati, India. This tunnel has a test section of square cross-section of 0.6 m × 0.6 m and a length of 2 m. It is capable of generating freestream velocities in the range of 0.1 m/s to 50 m/s. Here, flow velocity is measured using a pitot static tube connected to an electronic manometer. This measurement has an uncertainty of 0.3%. The experiments are conducted for a freestream velocity range of 5 m/s to 13 m/s. The freestream turbulence level inside the test section is examined using a hot wire anemometer [Model: HWCTA-AMB717, Make: Sunshine Measurements], and it is found to be 0.35% for the tested speed range.

Table 1 Key parameters used for the printing process

Parameters	Description
Layer thickness	0.08 to 0.12mm (For better surface finish)
Infill pattern type	Grid (to optimize object weight, strength, and printing time)
Infill density	40 to 50 % (Provides stiffness)
Infill speed	30 to 35 mm/s (Usually low for better surface finish)
No. of shells	3-4 (to improve strength of model)

Herein S5010 airfoil section is chosen for fabricating the wing models of different *AR*s 2.0 and 1.0. This airfoil was specially designed for wings flying at low *Re* speeds and to generate higher lift at a lower *AoA* range than a conventional airfoil. The S5010 profile has a maximum camber of 0.018*c* at 0.32*c*, and the maximum thickness is 0.098*c* at 0.276*c* (Selig et al., 1996). For the wing with an *AR* of 2.0, the chord length is 0.120 m, and the span is 0.240 m. Meanwhile, for the wing with an *AR* of 1.0, the chord length is 0.170 m, and the span is 0.170 m. These models, made from polylactic acid (PLA) material, are printed using a fused deposition modeling (FDM) technology-based 3D printing machine [Model: Pro2, Make: RAISE3D]. In the FDM process, a thermoplastic filament is heated and extruded layer by layer to create a three-dimensional object. This is to ensure that the models have a favorable surface finish and better structural stability. A series of assessments has been made on the basis of material layer height, feeding speed, and number of shells, as shown in Table 1. Accordingly, it has been noted that the printing composition of 0.08 - 0.12 mm layer height, 30 - 35 mm/s feed speed, and 3 - 4 nos. of shells produce a good surface finish and structural stability of the model (Ayrilmis, 2018). The models fabricated with this setup exhibit negligible aerodynamic deviation under low Reynolds number conditions, thereby minimizing any significant impact on the boundary layer.

In this study, the self-movable flap is made of a thin Mylar sheet of thickness 0.12 mm and is considered for mounting at various chord-wise locations ranging between 0.3*c* and 0.8*c* on the suction side of the wing surface. The flap width sizes are chosen from 0.12*c* to 0.20*c*, and the leading edge of the flap is attached to the wing surface using Polypropylene adhesive tape of thickness 30 µm. This configuration allows the flap to rotate freely about its leading edge at a fixed location. A tensile test is performed using a universal testing machine [Model: Acumen 12, Make: MTS systems corporation] for the Mylar sheet to estimate Young's modulus (E) for the calculation of flexural stiffness. For testing, a Mylar sheet with dimensions of 85 mm length, 18 mm width, and 0.12 mm thickness is used. The Young's modulus of the flap material is measured as 6.357 kN/mm^2 for the tested sample size. The flexural stiffness (EI) of this thin film is obtained as 16.477 N-mm^2 by the adopting procedure as described by Combes and Daniel (2003), indicating that the material has sufficient rigidity to resist deformation during the lifting process. The representation of flap span, chord size, and their position details on the wing surface are shown by a sketch in Fig. 2. In the initial phase of the flap experiments, four different flap span lengths are tested to study the three-dimensional effect on the flap

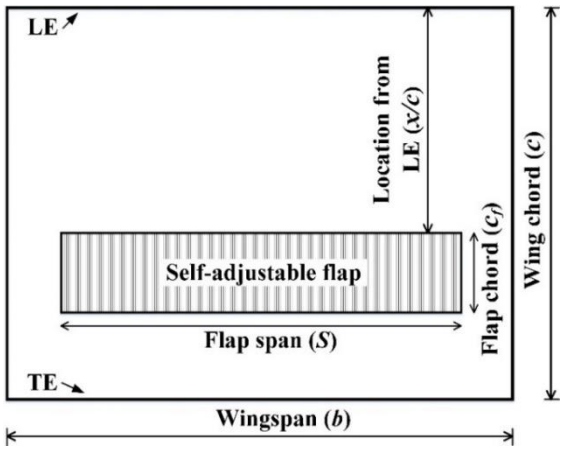

(a) top view

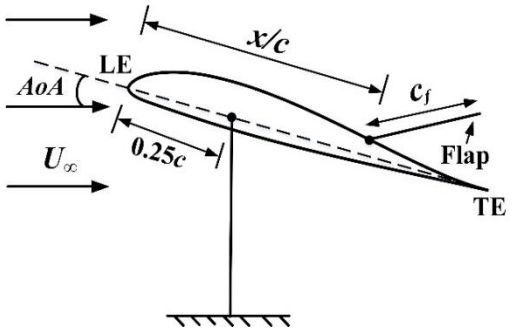

(b) side view

Fig. 2 Schematic representation of flap geometry details and its placement on the wing surface

dynamics for both the wing models. In the first arrangement, the flap span is extended over the entire span of the wing (S = 1.0b). For other configurations, the flap span is chosen as 0.9b, 0.8b, and 0.7b and placed on the wing surface in such a way that symmetry is maintained. Single and multiple flapped wing configurations are mounted on the force balance, as shown in Fig. 3.

Aerodynamic forces and moment acting on the models are measured using a three-component strain gauge-based force balance (Model: WBAL-00103, Make: Sunshine Measurements). This balance estimates lift, drag, and pitching moment with optimum load capacities of 10 N, 4 N, and 0.5 N-m, respectively. The resolution of the force balance, as specified by the manufacturer, is 0.001 N for lift and drag forces and 0.0001 N-m for a pitching moment. Furthermore, the uncertainty in the balance is less than ±3.0% for lift and pitching moment measurements and less than ±1.5% for drag measurements. The complete experimental setup for

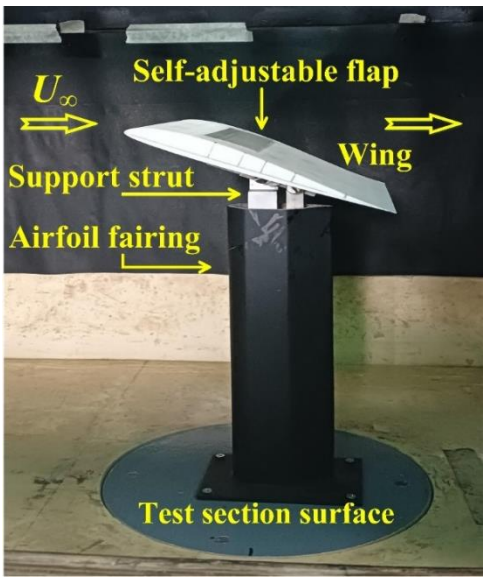

(a) Single flap configuration

(b) Multiple flaps configuration

Fig. 3 Mounting of a wing with attached flap on the force balance inside the test section

aerodynamic measurements on the wing is shown by the schematic in Fig. 4. Here, the balance system is mounted on the floor of the test section, and the model is affixed on the angle piece (model support plate), which is hinged at the top vertical bar of the balance. This support strut is covered by an airfoil-shaped fairing that is not connected to the balance mechanism. A fairing is a structure that provides streamlined flow due to its airfoil shape and reduces drag. It is fixed to a wooden plate, and it doesn't transmit any force to the balance's measuring mechanism. The strut passes through the fairing without contact and is directly connected to the balance system. The bottom portion of this bar is attached to the metric plate, which is linked to strain sensors through link elements. The pitch angle of the mounted model can be adjusted between –10° and 30° to the flow direction and is measured using a digital spirit level with an uncertainty of ± 0.1°. Additionally, the force balance system is equipped with a provision to adjust and set the angle of attack as required. To ensure accuracy, the digital spirit level measurements are cross-verified with the scale provided in the balance

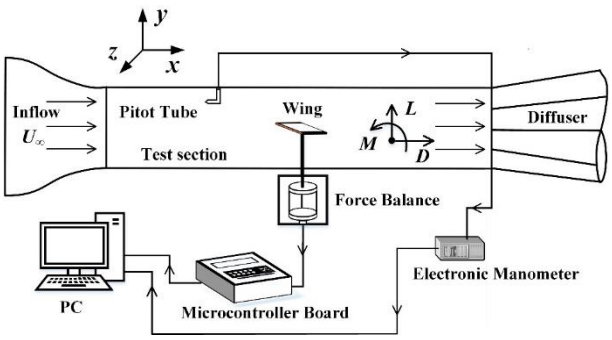

Fig. 4 Experimental setup

system. This dual approach ensured that the angle of attack is consistently and reliably measured throughout the experiments.

In order to assess the interference caused by the model support structure, an additional experiment is conducted without mounting the wing model on the balance. In this manner, the balance measures the drag force generated by the support strut structure (without the wing model). This value is then subtracted from the total drag values experienced by the wing model to eliminate the effect of interference from the support strut in the force measurement. Another essential parameter in the wind tunnel experiments is the blockage ratio, defined as the ratio of the wing's frontal area to the cross-sectional area of the test section. In the present study, this factor is found to be in the range of 0.56% to 3.52% when a wing of *AR* = 1.0 is tested at *AoA* from 4° to 26°. At the same time, it is observed to be between 0.55% and 2.74% for a wing of *AR* = 2.0 in the *AoA* range of 4° to 20°. As suggested in the literature, it is not required to incorporate blockage correction in the measurement when the blockage ratio values are less than 5% (Barlow et al., 1999; Chen & Liou, 2011; Jeong et al., 2018).

Moreover, validation of the present measurement setup has also been carried out before initiating the experiments on the wing with a self-adjustable flap. Since there is no experimental lift data available for the S5010 profiled wing of *AR* = 2.0 and 1.0 in the existing literature, hence it is validated with data from the infinite wing model for the same airfoil obtained by Selig et al. (1996). The results obtained in this study are for the S5010 airfoil-based infinite wing model at $Re = 6 \times 10^4$, and it is validated with Selig's experimental results, as shown in Fig. 5. The present results exhibit good agreement with reported data for the tested range of *AoA*, indicating the reliability of the measurement setup.

For error estimation in aerodynamic coefficient measurement, the standard deviation of the measured samples and subsequent standard error of the mean is estimated (Moffat, 1988). This force balance has a sampling frequency of 100 Hz, and sample acquisition was conducted over a duration of 20 seconds. Measurements were repeated five times at each *AoA*, maintaining consistency across experimental conditions, whether performed on the same day or on different days. The maximum standard errors of the mean are found to be

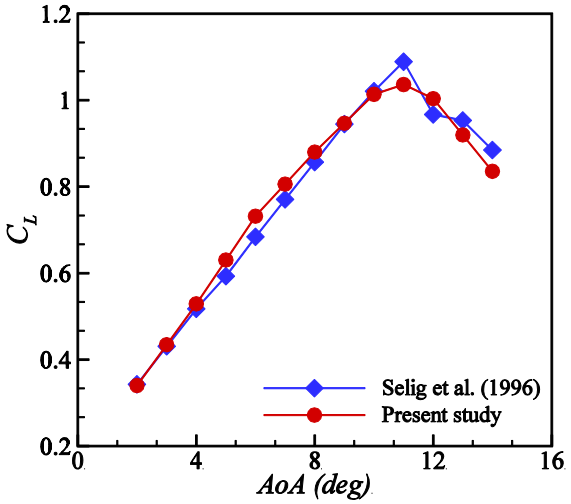

Fig. 5 Validation of lift of the present study with the reported data at $Re = 6 \times 10^4$

less than ±3.0 % for lift and moment measurement, while for drag, it is less than ±1.5 %. These estimated errors are represented by the error bars in the lift and drag curve for various flapped wing configurations of AR = 2.0 at Re of 1×10^5, as shown in Fig. 6.

3. Results and Discussion

Experiments are conducted to explore the effectiveness of a passive flap for the S5010 profiled wing of two different aspect ratios (AR = 2.0, 1.0) in the Re range of 6×10^4 to 1×10^5. The results of the investigation are discussed in two different sub-sections. The first sub-section discusses flap dynamics and analysis of parametric variation of flap span lengths to estimate the optimal flap span size. The next sub-section covers the discussion about the effect of different flap chord lengths and their chord-wise placement on the wing surface on the aerodynamic performance. Finally, the influence of AR and Re on the flap effectiveness is addressed.

3.1 Understanding of Flap Dynamics and Flap Span Effects

Initial wind tunnel experiments are carried out to obtain an overview of the fundamental behavior and set of possible flap designs for the existing wing configurations. In this phase, a thin Mylar sheet, emulating the covert feathers of the bird, is installed on the suction surface of the wing near the trailing edge. When the flapped wing is tested at a lower AoA, it is observed that the flap remains attached to the surface and has no influence on the wing's aerodynamics. This observation is illustrated in the schematic shown in Fig. 7a. However, as the AoA is increased, the flap begins to rise and adjusts itself to an equilibrium position, which eventually controls the flow separation (Fig. 7b). This is the reason these flaps are called as self-adjusting flaps. Such flaps do not require an actuation device to activate; however, the opening and closing actions of the flap are controlled by the flow surrounding the wing. Once the flow starts to separate from the trailing edge, reverse flow is bound to occur in this separation regime (Bechert et al., 1997). Under these

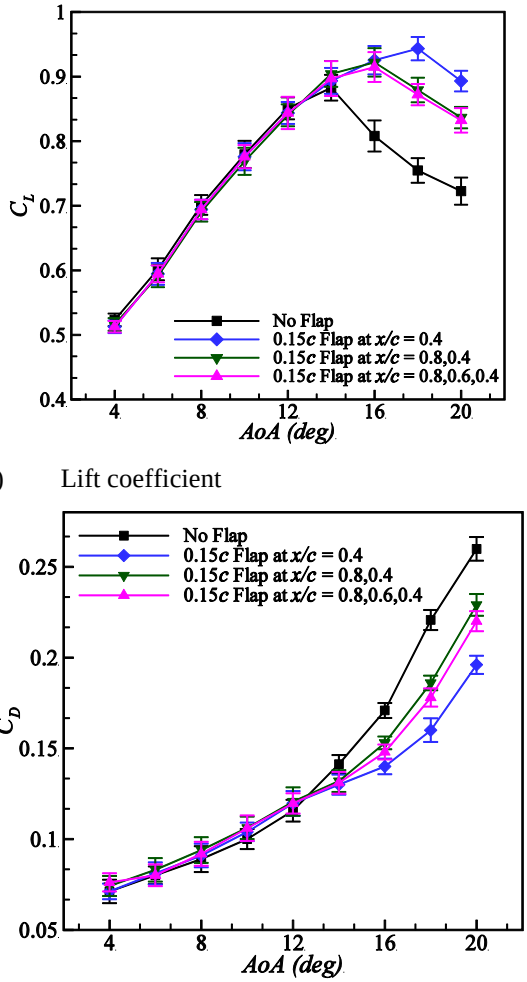

(a) Lift coefficient

(b) Drag coefficient

Fig. 6 Error analysis in the measurement of lift and drag for flap configuration of AR = 2.0

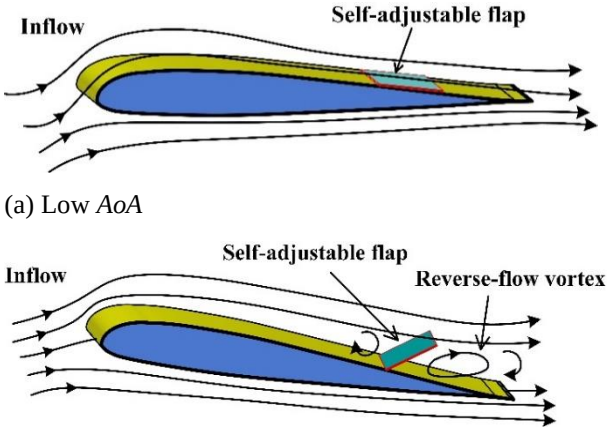

(a) Low AoA

(b) High AoA

Fig. 7 Schematic representation of self-adjusting movable flap behavior for (a) pre-stall and (b) post-stall zones

flow conditions, the flap begins to deploy passively as the recirculation bubble moves upstream for an increased AoA. Thus, it acts as a brake since it prevents the separation bubble region from spreading towards the

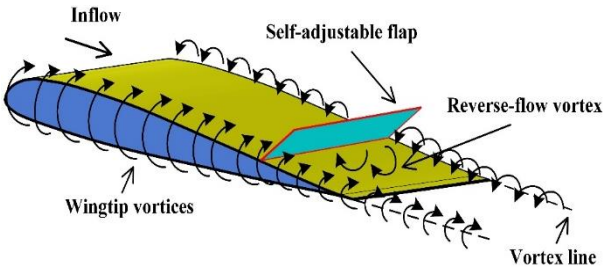

Fig. 8 Influence of wingtip vortices over flapped wing configuration

leading edge. Consequently, static pressure distribution on the suction surface upstream of the flap gets lower than that of the rear part of the flap (Meyer et al., 2007). This decrease of pressure on the suction surface upstream of the flap is beneficial to increase the lift at a higher *AoA*. As the present study deals with the finite wings, it is obvious that wingtip vortices will be present, as shown in Fig. 8. These wingtip vortices would alter the pressure distribution over the wing surface and flow over the flap. Therefore, it would be interesting to explore how the flapped wing's performance would change with decreasing flap span length along the wingspan.

In this regard, experiments are carried out on the wing of AR = 2.0 and 1.0 with a flapped configuration of reducing flap span sizes from 1.0b to 0.7b along the wing spanwise. The study is accomplished for flap width between 0.12c and 0.2c and its various chord-wise locations between 0.3c and 0.8c at the Re of 1 × 10^5. The lift coefficient corresponding to different flap span lengths for a flap chord of 0.15c at a location of 0.4c is presented in Fig. 9. For the clean wing of AR = 2.0, C_L increases with increasing *AoA* up to 14°; beyond that, it begins to decline (Fig. 9a). So, the stall angle is recorded close to 14°, and corresponding C_L is found as 0.88. In the case of AR = 1.0, the stall point is noted as 20°, and associated C_L is 0.65 at Re = 1 × 10^5 (Fig. 9b).

All flapped wing configurations exhibit the same lift characteristics as respective clean wings in the pre-stall region irrespective of any flap spanning size. Beyond the stall angle of the wing, all the flap configurations show a significant effect on the lift characteristics except the flap span of 1.0b. The flap spanning 100% of the wingspan (S = 1.0b) does not show any lift improvement, even in the post-stall region for any position and width of the flap. In the case of full-span flap configuration, the flap movement is obstructed by the downwash induced by wingtip vortices. So, the flap remains attached to the upper wing surface at low to high angles of attack; hence, it does not affect the aerodynamic performance of the wing. In contrast, this downwash effect is insignificant for an infinite or high aspect ratio wing, so full-span flaps work effectively and have been proven to be a performance enhancement effector (Bramesfeld & Maughmer, 2002; Liu et al., 2010).

Further, results reveal that as the span of the flap decreases, significant improvement in the lift and stall

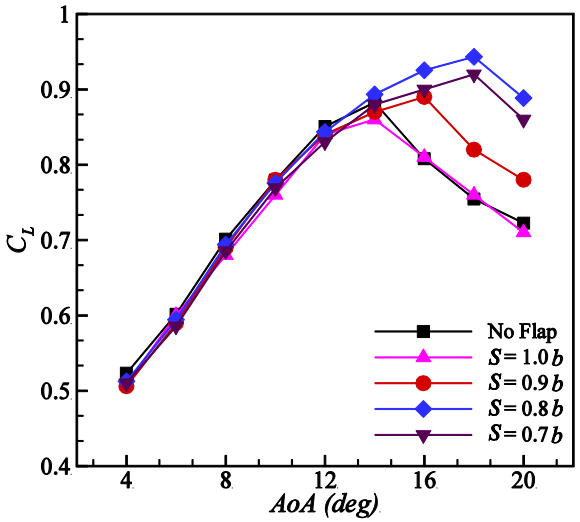

(a) AR = 2.0

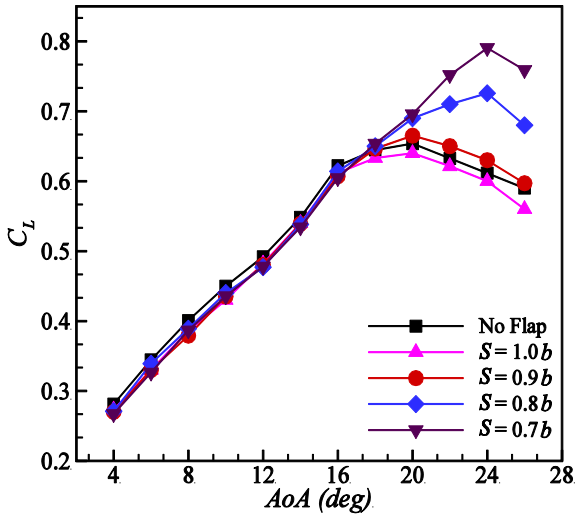

(b) AR = 1.0

Fig. 9 Lift characteristics corresponding to different flap span lengths for chord flap chord of 0.15c at location 0.4c for Re = 1 × 10^5

characteristics is observed for the configurations. When the flap span is 90% of the wingspan, the stall point increases to near 14% for AR = 2.0, and no improvement is seen for AR = 1.0 wings. As reported, the effect of downwash on the suction surface increases with the decrease in the wing AR (Mizoguchi & Itoh, 2013). Therefore, the effect of wingtip vortices is more pronounced on the flap motion of the AR = 1.0 model. For a flap span of 80 to 70 % of wingspan, stall angle increases up to 28% and 20%, respectively, in the case of AR = 2.0 and 1.0. These experimental results indicate that by reducing the flap span, it is possible to minimize the effect of downwash acting on the flap dynamics, thereby contributing to higher lift generation. On the other side, greatly reducing the span of the flaps also reduces the contribution to lift generation for the post-stall region. In the current study, the optimal flap span length is found as 80% of wingspan (S = 0.8b) for AR = 2.0 and 70% of wingspan (S = 0.7b) for AR = 1.0, which is the same for all the flap chord sizes and their locations. The difference

in optimal flap span length is expected to be primarily caused by variation in wingtip vortices, which induce downwash on the upper wing surface. This downwash can alter the pressure distribution over the wing's surface and affect flap movement, thereby impacting the flap's effectiveness (Mizoguchi & Itoh, 2013; Altman & Allemand, 2016).

3.2 Analysis of Flap Chord Sizes and Positions

Since self-adjusting flaps are raised by reverse flow, the flap must be light in weight and positioned optimally on the wing so that it can respond properly to the reverse flow. Essentially, the weight is affected by two factors, namely, the flap material and its size. Here, the flap material and its thickness are not changed during testing. Therefore, to figure out the optimal flap size and position for the current models, experiments are carried out for different flap chord lengths ranging from 0.12*c* to 0.2*c* at *Re* of 1×10^5. These flap sizes are examined for different chord-wise flap positions starting from near the trailing edge at 0.8*c* and progressing upstream to 0.3*c*. The effect of these locations and flap dimensions are discussed in this section.

3.2.1 Lift Characteristics

The measured lift coefficients corresponding to various flap chord lengths (0.12*c*, 0.15*c*, 0.2*c*) and their positions (*x/c* = 0.8, 0.6, 0.4) for *AR* = 2.0 wing are presented in Fig. 10. The analysis of results show that the lift curve remains the same in the pre-stall zone for both clean and flapped models of any given flap chord length and its location. Meanwhile, for the post-stall region, all the flapped wings reveal improvement in the lift and stall characteristics compared to the clean model. In the case of configuration with attached flap length of 0.12*c* at *x/c* = 0.8, 0.6, 0.4, the stall angle has been noticed to be increased by 14% (Fig. 10a). Further, the C_L increases by 15% at *AoA* = 16°. Changing the flap location upstream does not provide any advantages in terms of lift or stall for this configuration. When the chord is 0.15*c*, flapped wing shows smooth stall characteristics, and the stall angle rises by 22% for flap locations at *x/c* = 0.6, 0.4 (Fig. 10b). For the same locations, C_L improves by approximately 27% at *AoA* = 18°. The flap mounting at *x/c* = 0.6, 0.4 has better lift and stall characteristics than the flap attached close to the trailing edge at *x/c* = 0.8.

A similar test has been performed with a chord length of 0.2*c*, and the results show that the stall angle increases by 22% at *x/c* = 0.6 and by 14% at other places (Fig. 10c). An increase in flap chord length from 0.12*c* to 0.15*c* has shown a substantial improvement in both lift and stall angle. The flap size of 0.12*c* may be less effective in obstructing the progression of reverse flow in the upstream of flap due to its lighter weight, which can lead to a loss of lift and an earlier stall. However, when the flap size increases from 0.12c to 0.15c, the ability to obstruct the spreading reverse flow is expected to improve, which may contribute to improving lift and stall angle. Further, increasing the flap chord from 0.15*c* to 0.2*c* resulted in an almost identical increase in lift on the wing. Thus, the optimal range of flap size for an *AR* = 2.0 wing is found to be higher than 0.12*c* and lower than 0.2*c* for better performance enhancement. In addition, flap positions show a substantial effect on lift and stall behaviors. Configurations with attached flap at *x/c* = 0.6 or 0.4 provide a higher value of lift or stall angle than other locations, irrespective of any flap chord sizes.

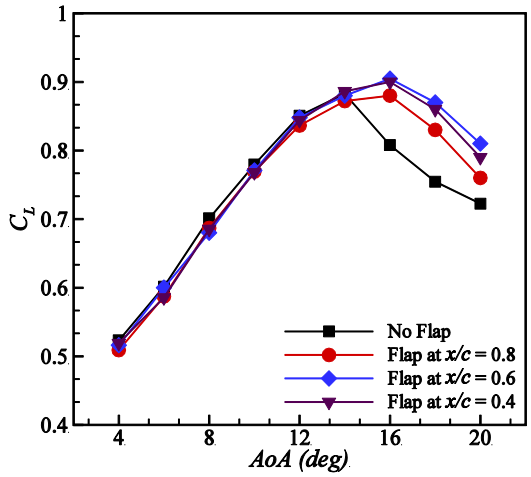

(a) Flap chord-size = 0.12*c*

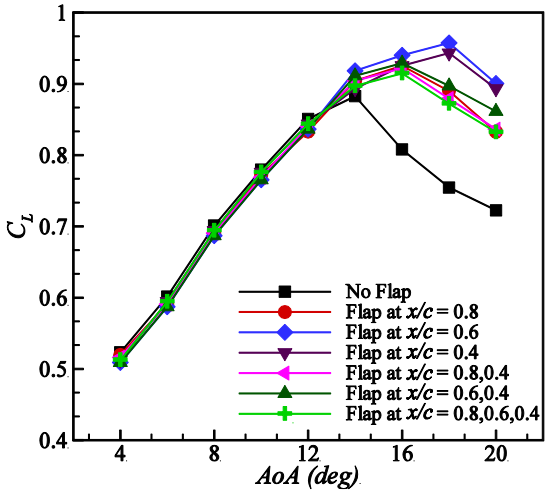

(b) Flap chord-size = 0.15*c*

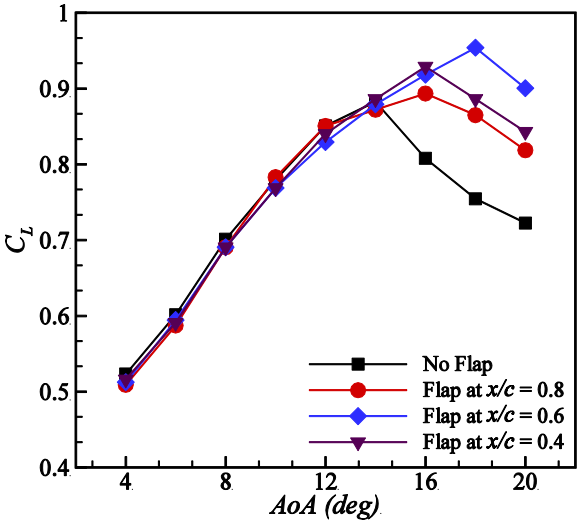

(c) Flap chord-size = 0.2*c*

Fig. 10 Lift characteristics of an *AR* = 2.0 wing with various flap chord sizes and positions at *Re* = 1×10^5

Moreover, this experiment is also extended to study the effect of multiple flaps on the wing performance for the current *Re*. For this, three sets of flap configurations are explored. The first configuration has two flaps, one closer to the mid-chord (0.4*c*) and the other near the trailing edge (0.8*c*). In the second arrangement, both flaps are located around the midpoint of the chord (*x/c* = 0.4, 0.6), and in the final arrangement, the three flaps are placed at *x/c* = 0.8, 0.6, 0.4. The results of *AR* = 2.0 wing with arrangements of double and triple flaps of size 0.15c are presented in Fig. 10b. It is observed that all multiple flap configurations exhibit higher post-stall lift and increase in stall angle than the clean wing. Here, the stall angle increases by 14%, and lift rises by 15% at *AoA* = 16°, which is the same for both double and triple flap setups. However, this gain in lift and stall is lower when compared to the increase obtained by the single-flapped wing for a location of 0.4*c* or 0.6*c*. In single-flapped configurations, the flap is expected to more effectively obstruct reverse flow in the separation region and maintain attached flow upstream of the flap, which can lead to enhanced lift and delayed stall. In contrast, the introduction of multiple flaps can cause additional disturbances in the flow, potentially leading to a premature transition to turbulence (Arivoli & Singh, 2016). This transition may destabilize the separation bubble, making it more challenging to control reverse flow and adversely affecting the pressure distribution over the wing surface. Consequently, double or triple-flapped configurations may exhibit less lift enhancement and stall delay than a single-flapped arrangement. Further, the same experiments were also performed on other flap chord sizes, such as 0.12*c* and 0.2*c*, for the same wing, and similar results were obtained as with the 0.15*c* case. Thus, single-flapped configurations show better lift and stall enhancements over double or triple-flapped arrangements for all flap chord sizes. Similar lift and stall behavior reductions were observed by employing double self-adaptive flaps compared to a single flap for the same rectangular flat plate wing (Arivoli & Singh, 2016).

A similar flap experiment is also carried out for a wing of *AR* = 1.0 to study the effect of flap chord size and its locations on aerodynamic performance. In these tests, the flap is initially considered at a downstream location of *x/c* = 0.8 and then moved to other upstream locations such as 0.6, 0.5, 0.4, and 0.3. Figure 11 shows lift coefficient variation attributed to different flap chord sizes (0.12*c*, 0.15*c*, 0.2*c*) and their placement at $Re = 1 \times 10^5$. The lift curve shows that stall occurs at 20° for the clean wing. Similar to the *AR* = 2.0 flap model, all flapped configurations have approximately the same lift as the clean wing in the pre-stall region. The flaps at locations *x/c* = 0.8 and 0.6 do not provide significant improvements in the lift and stall angle for the *AR* = 1.0 wing. For a flap of 0.12*c* size at upstream positions *x/c* = 0.5, 0.4, 0.3, the stall point increases by 10% over the clean model (Fig. 11a). When the flap size increases from 0.12*c* to 0.15*c*, the stall angle increases by 20% at *x/c* = 0.4 (Fig. 11b). Further increase in flap size does not provide any benefit for improving lift and stall than the flap of 0.15*c* (Fig. 11c). Moreover, moving the flap positions on the model from the trailing edge towards upstream shows a beneficial

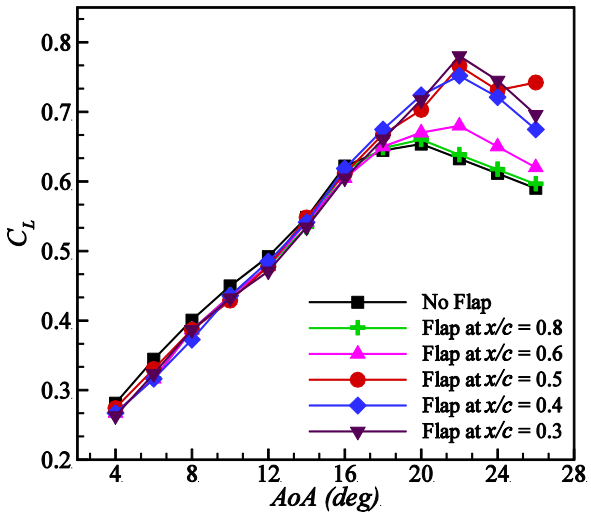

(a) Flap chord-size = 0.12*c*

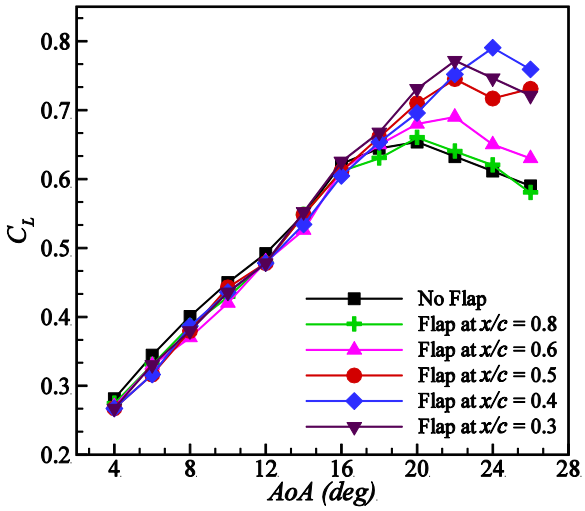

(b) Flap chord-size = 0.15*c*

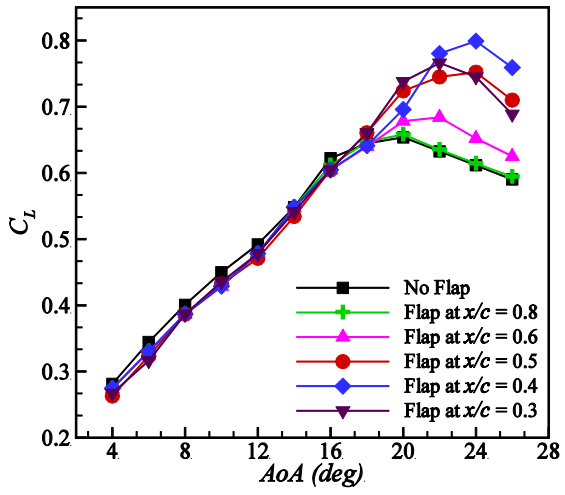

(c) Flap chord-size = 0.2*c*

Fig. 11 Lift characteristics of an *AR* = 1.0 wing with various flap chord sizes and positions at $Re = 1 \times 10^5$

effect on the post-stall lift characteristics. For the *AR* = 1.0 model, a configuration with a flap of 0.15*c* at *x/c* = 0.4 on the model demonstrates better lift or stall behavior

compared to other flap sizes and locations. The experiments are also performed for multiple flaps on the wing to evaluate the performance enhancement capacity in the case of a low aspect ratio wing (AR = 1.0). Similar to the AR = 2.0 model, all double or triple flap configurations show higher post-stall lift values and stall angles than the baseline case. However, this increase in the lift is lower when compared to the lift obtained by the single-flapped arrangement.

The present analysis demonstrates that variations in wing AR result in significant changes in lift and stall behaviors. For the clean wing, with a decrease in the aspect ratio from 2.0 to 1.0, the maximum lift coefficient (C_{Lmax}) decreases by close to 26% at $Re = 1 \times 10^5$, while the associated stall angle increases from 14° to 20°. Hence, the C_{Lmax} of the wing decreases with a decrease in AR. Similar behavior of C_{Lmax} as a function of AR was also observed for the flat plate wings ($1.0 \leq AR \leq 3.0$; $6 \times 10^4 \leq Re \leq 200 \times 10^3$) (Pelletier & Mueller, 2000). In the case of flap configurations, AR also shows a substantial effect on the flap effectiveness. Reducing the AR of the wing reduces flap span size to work effectively by eliminating the effect of wing tip vortices. Further, the optimal flap location is also varying with the AR. For AR = 2.0, the positioning of the flap between the mid-chord and trailing edge locations has a favorable influence on lift and stall characteristics for all flap chord sizes. In the case of AR = 1.0, the positive effect of the flap is noticed only for the upstream location of the mid-wing. However, Altman & Allemand (2016) observed that changing the AR from 7.0 to 4.0 had no major effect on flap effectiveness for high AR wings. In terms of lift coefficient, the AR = 2.0 wing appears to be more sensitive to parametric variations in flap chord lengths and its positions for a given Re than AR = 1.0.

3.2.2 Drag Characteristics

The influence of single or multiple flap arrangements on the drag characteristics of the wing is estimated at $Re = 1 \times 10^5$, as presented in Fig. 12. Figure 12a shows the variation of C_D as a function of AoA for AR = 2.0 wing with different flap positions of chord size 0.15c. The drag value continues to increase with an increasing AoA, which is the same for both clean and flapped configurations. However, the value of C_D rises gently with an angle for a lower AoA ($AoA \leq 12°$), while at higher angles, the drag force rises rapidly. Here, the plotted drag data is the total drag acting on the wing, which is a combination of profile drag (skin friction and form drag; arising due to viscous effect) and induced drag (resulting from wingtip vortices). It has been noted that, for streamlined bodies at lower angles, the values of form drag and induced drag are small, which means that the majority of the drag force is due to skin friction drag (Anderson, 2011). This concept helps to explain the lower rate of rising C_D for lower AoA. However, as the AoA increases, the flow begins to separate from the upper surface of the wing. As a result, form drag begins to increase due to flow separation, and hence, the C_D increases rapidly at high AoA.

The influence of flap arrangement on the drag force is less significant for the pre-stall region but more significant for the post-stall angles. All the flapped configurations

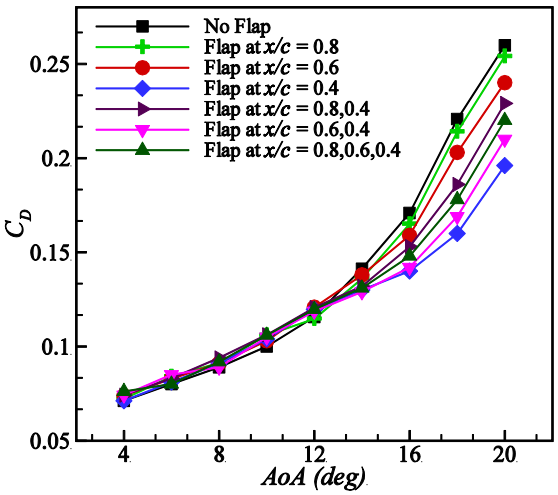

(a) AR = 2.0

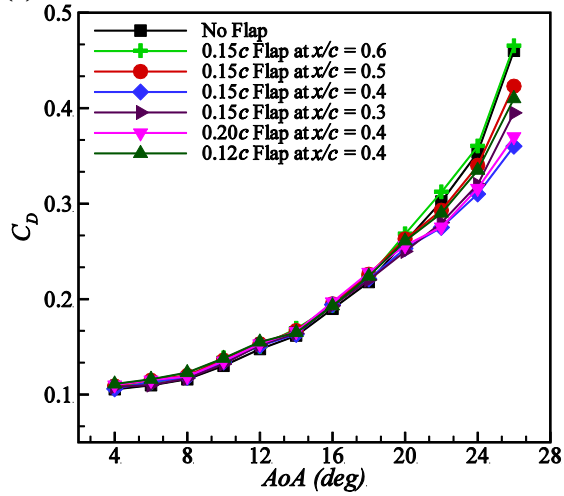

(b) AR = 1.0

Fig. 12. Drag characteristics of different flapped wing configurations at $Re = 1 \times 10^5$

show significantly low values of drag against the baseline case, except for the flap location of 0.8c. The drag curve for a flap position near the trailing edge (x/c = 0.8) is similar to that of a clean wing. Further, double (0.4c and 0.8c, 0.4c and 0.6c) and triple (0.4c, 0.6c, 0.8c) flapped configurations exhibit relatively higher drag coefficients as compared to the flap location of 0.4c (Fig. 12a). The addition of multiple flaps can cause additional flow disturbances, leading to premature transition into turbulence (Arivoli & Singh, 2016). This transition destabilizes the separation bubble, resulting in increased pressure drag. Consequently, double or triple-flapped configurations exhibit higher drag than the single-flap configuration. Flap chord size also reveal significant effects on the post-stall drag behavior. As the flap chord is increased from 0.12c to 0.15c, the magnitude of the drag coefficient for the post-stall zone decreases. However, with a further increase, i.e., from 0.15c to 0.2c, the drag force does not change significantly. A similar experiment is also carried out for estimating the drag force for AR = 1.0 wing with different flap sizes and their arrangements; results are presented in Fig. 12b. Drag coefficients for the pre-stall region are unaffected by the presence of flap, which is the same for all flaps configurations. For post-

stall angles, flap placement between the leading edge to the mid-wing chord has shown a lower drag value than the un-flapped one. Similar drag reduction was observed for the NACA0012 airfoil attached to the passively flexible thin fin close to the leading edge (x/c = 0.1, 0.2) in the post-stall zone (Liu et al., 2010). In contrast, the configuration with flap placement downstream of the mid-wing exhibits a drag curve similar to that of a clean wing, even in the post-stall region. Similar to AR = 2.0, the double and triple flap arrangement models also show higher drag than the single flap at x/c = 0.4. Further, a flap of 0.12c chord length reveals a higher drag value than a chord of 0.15c and 0.2c for all the locations. Compared to AR = 2.0 flap configurations, changing flap parameters such as cord, location, and flap numbering have less effect on the drag characteristics for AR = 1.0.

3.2.3 Moment Characteristics

The pitching moment data is obtained at about a quarter chord (*0.25c*) of the wing for all the flap configurations at $Re = 1 \times 10^5$. Here, the moment coefficients as a function of *AoA* for AR = 2.0 and 1.0 wing with different flap chord sizes and their positions are presented in Fig. 13. For the clean wing, the magnitude of $C_{M,0.25c}$ decreases to negative values with increasing angle up to 14°, and after this angle, an increasing trend is seen for AR = 2.0 (Fig. 13a). Also, in case AR = 1.0, the pitching moment curve decreases till 20°, then an increasing trend is noticed (Fig. 13b). The rise in the moment curve following a specific angle is related to the reduction in lift. As it has been noted that the behavior of the lift curve alters as it gets near the stall angle, a similar trend has also been noted for the moment curve. It also changes its behavior near the stall point. Similar moment behavior associated with lift characteristics was observed for flat plate wings of various planforms (Okamoto & Azuma, 2011). The significance of the negative pitching moment refers to the fact that when the *AoA* rises, it tends to rotate the wing towards its equilibrium position to offset the disturbance caused by the *AoA*. Also, it was emphasized that the slope of the moment curve must be negative for the static longitudinal stability of aircraft (Nelson, 1998). In this study, the moment slope is estimated from the linear region of the curve and is found in negative values as -0.0104 /*deg* and -0.0072/*deg* for the base wing of AR = 2.0 and 1.0, respectively.

Further, the moment characteristics in the pre-stall region are unchanged by using this passive flap, irrespective of its size and position for both models. In contrast, the flap affects the moment behavior significantly after the stall point. All the flap configurations show more negative pitching values for the post-stall angles than the baseline. This indicates that the pitch-down tendency of the flapped wing is higher than the un-flapped one in the post-stall zone. A flap at locations of x/c = 0.6 or 0.4 exhibits a more negative magnitude of $C_{M,0.25c,}$ than other flap arrangements for AR = 2.0 (Fig. 13a). Moreover, single-flap configurations show more pitch-down tendencies as compared to the double or triple-flapped wings. When the flap chord length increases from 0.12c to 0.15c, the post-stall moment rises in the negative magnitude. In contrast, a further increase in chord size,

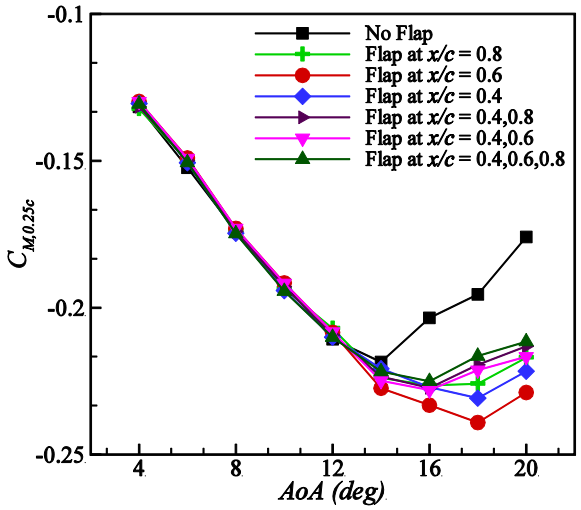

(a) AR = 2.0

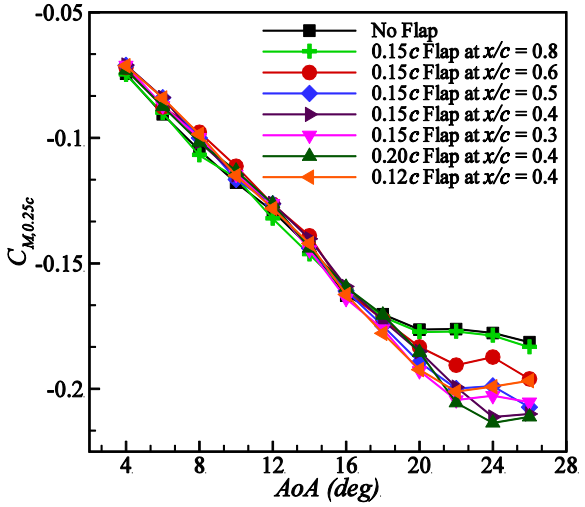

(b) AR = 1.0

Fig. 13 Pitching moment characteristics of different flapped wing configurations at $Re = 1 \times 10^5$

such as from 0.15c to 0.2c, does not affect the moment coefficient. For AR = 1.0 models, the moment curve is unaffected by the flap position close to the trailing edge (x/c = 0.8) but is affected by the upstream or mid-wing position of the flaps (Fig. 13b). Configuration with flap at x/c = 0.4 shows more pitch-down tendency as compared with other flap locations at high *AoA*. Similar to AR = 2.0, double or triple flap arrangement exhibits a lower negative value of $C_{M,0.25c,}$ than single. Moreover, increasing the flap size from 0.12c to 0.15c improves the more negative magnitude of the moment, while expanding the size above 0.15c does not affect the moment behavior. Similar to lift and drag behavior, the moment characteristics of the AR = 2.0 flap configurations are more sensitive to changing flap parameters than those of a low AR wing.

3.3 Effect of Aspect Ratio and Reynolds Number on Flap Effectiveness

The present analysis demonstrates that variations in wing AR result in significant changes in lift and stall behaviors. For the clean wing, with a decrease in the AR from 2.0 to 1.0, C_{Lmax} decreases by close to 26% at Re = 1

$\times 10^5$, while the associated stall angle increases from 14° to 20°. Hence, the C_{Lmax} of the wing decreases with a decrease in *AR*. This can be justified by the classical theory. As per the conventional theories for the prediction of aerodynamic lift for low *AR* wings, the lift generation has two sources: linear and nonlinear (Gabriel & Mueller, 2004). Linear lift is described by the potential theory, where lift is associated with circulation around a wing, while the nonlinear lift component appears from the presence of wing tip vortices. When the wing *AR* is reduced, the potential theory-based lift reduces because of the strong downwash caused by the tip vortices (Mizoguchi & Itoh, 2013). Thus, with a decreasing wing *AR*, the total lift decreases. Additionally, these tip vortices can re-energize the slower-moving boundary layer on the suction surface of the wing and thereby delay the flow separation in the downstream direction (Mizoguchi & Itoh, 2013; Karasu et al., 2018). These dynamics may potentially increase the stall angle for the lower *AR* wings. Moreover, C_{Lmax} increases with increasing Re for both the AR, as shown in Fig. 14. Similar behavior of C_{Lmax} as a function of AR and Re was also observed for the flat plate wings ($1.0 \leq AR \leq 3.0$; $6 \times 10^4 \leq Re \leq 2 \times 10^5$) (Pelletier & Mueller, 2000). In the case of flap configurations, AR also shows a substantial effect on the flap effectiveness. Reducing the AR of the wing reduces flap span size to work effectively by eliminating the effect of wing tip vortices. Further, the optimal flap location is also varying with the AR. For AR = 2.0, the positioning of the flap between the mid-chord and trailing edge locations has a favorable influence on lift and stall characteristics for all flap chord sizes. In the case of AR = 1.0, the positive effect of the flap is noticed only for the upstream location of the mid-wing. However, Allemand observed that changing the AR had no major effect on flap effectiveness for high AR wings (Altman & Allemand, 2016). In terms of performance (lift, drag, moment), the AR = 2.0 wing appears to be more sensitive to parametric variations in flap chord lengths and its positions for the same Re than AR = 1.0.

Moreover, no significant effect of Re on the flap dynamics is observed in the pre-stall region. Therefore, aerodynamic coefficients for pre-stall angles remain unchanged with varying Re from 6×10^4 to 1×10^5. But, this self-adjustable flap responds differently at various Re for particular flap size and their position for post-stall angles, as presented in Fig. 14. For AR = 2.0 flap configurations, the C_{Lmax} increases with increasing Re from 6×10^4 to 8×10^4 for all the cases (Fig. 14a). However, for Re between 8×10^4 and 1×10^5, the magnitude of C_{Lmax} is either almost constant or decreases with Re. With an increase in Re, the reverse flow momentum increases, which creates higher flap displacement and more lift to be produced. However, after a certain Re limit, the same flap is unable to resist these additional forces arising from increased velocity in the recirculation zone at some locations, causing the effect of a flap on the contribution of lift generation to be reduced. On the other hand, the positive influence of Re is observed on the C_{Lmax} for all flapped configurations of AR = 1.0 (Fig. 14b). As Re increases from 6×10^4 to 1×10^5, the

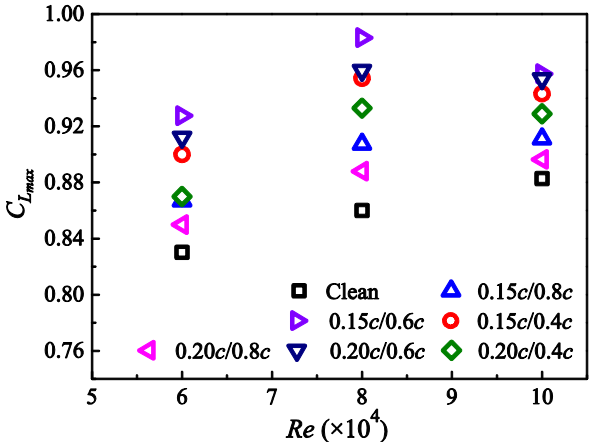

(a) *AR* = 2.0

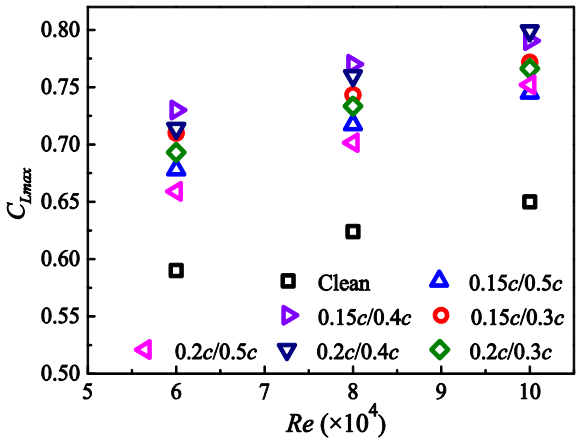

(b) *AR* = 1.0

Fig. 14 Maximum lift characteristics of different flap configurations wings at various *Re*

C_{Lmax} exhibits improvement for both chord lengths, 0.15*c* and 0.2*c*.

Based on the above observation, the behavior of C_{Lmax} as a function of *Re* shows a difference for both *AR* configurations, even while keeping the same flap chords and their placement. Thus, in order to obtain a positive response from the flap under different *Re*, flap size, position, and material will need to be changed. Similar flap behavior with varying *Re* was reported by Kernstine et al. (2008). In the case of drag coefficients, when the *Re* is increased from 6×10^4 to 1×10^5, post-stall drag data reduces for all flap configurations of *AR* = 2.0. While, for *AR* = 1.0 configurations, no significant effect of varying *Re* from 8×10^4 to 1×10^5 is noticed on the drag curve. For the pitching moment, it is found that the pitching moment values of the flapped wing of *AR* = 2.0 become more negative with increasing *Re*. Hence, the pitch-down tendency of the flapped wing rises with increasing *Re* in the post-stall region. At the same time, no significant effect of *Re* on moment characteristics is noted for the flapped *AR* = 1.0 model, even at a higher *AoA*. Thus, it is evident that the impact of varying *Re* on flap effectiveness reduces as the wing *AR* decreases.

4. CONCLUSIONS

This study is focused on investigating the feasibility of a self-adaptive movable flap on low *AR* wings and exploring flap effectiveness in various aspects, including flap span, chord length, and chord-wise placement for the MAV application. In this regard, the experiments are conducted with a S5010 profiled wing of two different *AR*s, 2.0 and 1.0, in the presence of a flap for the *Re* range of 6×10^4 to 1×10^5. Three different flap chord length setups, 0.12*c*, 0.15*c*, and 0.2*c*, have been tested for various chord-wise positions between 0.8*c* and 0.3*c*. Moreover, flap span size also varied from 1.0b to 0.7b in order to study the effect of tip vortices on flap effectiveness. The studies show that all flap configurations exhibit performance curves similar to a clean wing for the pre-stall region at a given *Re*. The flap spanning 100% of the wingspan does not provide any beneficial effect on the wing performance, even at a high *AoA*. When the flap span shrinks from both sides towards the wing center line, the influence of downwash on the flap motion is reduced, contributing more to lift generation. The best performance improvement is obtained when the flap covers 80% of the wingspan for *AR* = 2.0, and it is around 70% of the span in the case of *AR* = 1.0.

The flapped wing configurations reveal higher stall angle and post-stall lift coefficients than baseline in most cases. Initially, when the flap chord size increases from 0.12*c* to 0.15*c*, it enhances the lift and stall characteristics for both models. Further increases in flap size, such as 0.15*c* to 0.20*c*, do not provide any additional improvement in performance for all locations. The optimal location of this self-adjustable flap also varies with the *AR* of the wing. For *AR* = 2.0, the flap locations between 0.6*c* and 0.4*c* exhibit better performance than the other locations. Meanwhile, for *AR* = 1.0, better enhancement is observed for a flap location of *x/c* = 0.4, and no significant effect of the flap is noticed for a flap position downstream of a mid-wing chord. Multiple-flap configurations have a relatively lower lift-enhancing capability than single-flapped models in some locations. Further, in most cases, post-stall drag reduction is observed for flapped wings than a clean model, which is the same for both *AR*s. However, double or triple-flapped configurations show a lower drag value than baseline but higher than single flap in the post-stall region. When the flap chord is increased from 0.12*c* to 0.15*c*, the drag and moment characteristics improve, but an increase above 0.15*c* provides no beneficial effect. In the case of pitching moment, flaps do not change the longitudinal stability of the wing for pre-stall angles while increasing the pitch-down tendency of the wing in the post-stall region. The effect of *Re* on the flap effectiveness decreases with decreasing wing *AR*. Furthermore, the aerodynamic performance parameters of a flapped wing of *AR* = 2.0 appear to be more sensitive to parametric variations in flap chord length and its positions for the same *Re* than *AR* = 1.0. Overall, these experiments identify the optimal size and attachment location of a flexible flap on a low *AR* wing to delay stall, enhance lift, and reduce drag compared to a wing without a covert flap. Therefore, this passive flap can be a valuable device for improving the flying performance and maneuverability of MAVs. The present study can be extended to conduct particle image velocimetry (PIV) experiments on the flapped wing configurations to visualize and analyze the flow field around the flap. This approach could provide a more detailed understanding of the complex flow structures, such as separation, reverse flow, and vortex formation, which significantly affect the effectiveness of a self-adjusting flap.

ACKNOWLEDGEMENT

The first author is thankful to the Indian Institute of Technology Guwahati, India, for the scholarships during the period of study.

CONFLICT OF INTEREST

There is no conflict of interest related to the affiliation or involvement of any organization or any entity with a financial or nonfinancial interest in the subject matter or materials discussed in this manuscript.

AUTHORS CONTRIBUTION

Anand Verma: Conceptualization, Technical Insights, Experimental Design, Experimentation, Data Collection, Data Analysis, Visualization, Validation, Results Interpretation, Writing - Original Draft, Writing - Review & Editing. **Vinayak Kulkarni:** Conceptualization, Supervision, Technical Insights, Visualization, Data Collection, Data Analysis, Validation, Results Interpretation, Resources, Funding Acquisition, Writing - Review & Editing. **Sachin Shinde:** Conceptualization, Supervision, Technical Insights, Visualization, Data Collection, Data Analysis, Validation, Results Interpretation, Writing - Review & Editing.

REFERENCES

Altman, A., & Allemand, G. (2016, January 4-8). *Post-stall performance improvement through bio-inspired passive covert feathers*. 54th AIAA Aerospace Sciences Meeting, California, USA. https://doi.org/10.2514/6.2016-2042

Anderson, J. D. (2011). *Fundamentals of Aerodynamics.* 5th Edition, McGraw–Hill, New York.

Arivoli, D., & Singh, I. (2016). Self-adaptive flaps on low aspect ratio wings at low Reynolds numbers. *Aerospace Science and Technology*, *59*, 78–93. https://doi.org/10.1016/j.ast.2016.10.006

Arivoli, D., Singh, I., & Suriyanarayanan, P. (2020). Rudimentary emulation of covert feathers on low-ar wings for post-stall lift enhancement. *AIAA Journal*, *58*(2), 501–516. https://doi.org/10.2514/1.J058562

Ayrilmis, N. (2018). Effect of layer thickness on surface properties of 3D printed materials produced from wood flour/PLA filament. *Polymer Testing*, 71, 163-166. https://doi.org/10.1016/j.polymertesting.2018.09.009

Azuma, A. (1992). *The Biokinetics of Flying and Swimming*. Springer Tokyo, Japan. https://doi.org/10.1007/978-4-431-68210-3

Baljit, S. S., Saad, M. R., Nasib, A. Z., Sani, A., Rahman, M. R. A., & Idris, A. C. (2017). Suction and blowing flow control on airfoil for drag reduction in subsonic flow. *Journal of Physics: Conference Series*, *914*(1). https://doi.org/10.1088/1742-6596/914/1/012009

Barlow, J. B., Rae, W., & Pope, J. A. (1999). *Low-Speed Wind Tunnel Testing*. 3rd Edition, John Wiley & Sons, Inc, New York. https://doi.org/10.1063/1.3061735

Bechert, D. W., Bruse, M., Hage, W., & Meyer, R. (1997, June 29- July 02). *Biological surfaces and their technological application - Laboratory and flight experiments on drag reduction and separation control*. 28th AIAA Fluid Dynamics Conference, Snowmass Village, CO, U.S.A. https://doi.org/10.2514/6.1997-1960

Bramesfeld, G., & Maughmer, M. D. (2002). Experimental investigation of self-actuating, upper-surface, high-lift-enhancing effectors. *Journal of Aircraft*, *39*(1), 120–124. https://doi.org/10.2514/2.2905

Chen, T. Y., & Liou, L. R. (2011). Blockage corrections in wind tunnel tests of small horizontal-axis wind turbines. *Experimental Thermal and Fluid Science*, *35*(3), 565–569. https://doi.org/10.1016/j.expthermflusci.2010.12.005

Combes, S. A., & Daniel, T. L. (2003). Flexural stiffness in insect wings I. Scaling and the influence of wing venation. *Journal of Experimental Biology*, *206*(17), 2979–2987. https://doi.org/10.1242/jeb.00523

Cravero, C. (2017). Aerodynamic performance prediction of a profile in ground effect with and without a gurney flap. *Journal of Fluids Engineering, Transactions of the ASME*, *139*(3), 1–15. https://doi.org/10.1115/1.4035137

Gabriel, E. T., & Mueller, T. J. (2004). Low-aspect-ratio wing aerodynamics at low Reynolds number. *AIAA Journal*, 42(5), 865-873. https://doi.org/10.2514/1.439

Gad-el-Hak, M., & Pollard, A. (1998). *Flow control: Fundamentals and practices*. Springer Berlin Heidelberg. https://doi.org/10.1007/3-540-69672-5

Gerakopulos, R., Boutilier, M. S. H., & Yarusevych, S. (2010, June 28 - July 01). *Aerodynamic characterization of a NACA 0018 airfoil at low Reynolds numbers*. 40th AIAA Fluid Dynamics Conference, Chicago, Illinois. https://doi.org/10.2514/6.2010-4629

Hao, L., Gao, Y., & Wei, B. (2022). Experimental investigation of flow separation control over airfoil by upper surface flap with a gap. *International Journal of Aeronautical and Space Sciences*, *23*(5), 859–869. https://doi.org/10.1007/s42405-022-00488-x

Jeong, H., Lee, S., & Kwon, S. D. (2018). Blockage corrections for wind tunnel tests conducted on a Darrieus wind turbine. *Journal of Wind Engineering and Industrial Aerodynamics*, *179*, 229–239. https://doi.org/10.1016/j.jweia.2018.06.002

Karasu, I., Özden, M., & Genç, M. S. (2018). Performance assessment of transition models for three-dimensional flow over NACA4412 wings at low Reynolds numbers. *Journal of Fluids Engineering, Transactions of the ASME*, *140*(12), 1–15. https://doi.org/10.1115/1.4040228

Kernstine, K. H., Moore, C. J., Cutler, A., & Mittal, R. (2008, *January 1-9*). *Initial characterization of self-activated movable flaps, "Pop-up feathers."* 46th AIAA Aerospace Sciences Meeting and Exhibit, Reno, Nevada. https://doi.org/10.2514/6.2008-369

Kim, S. H., Hong, W., & Kim, C. (2007). Separation control mechanism of airfoil using synthetic jet. *Journal of Mechanical Science and Technology*, *21*(9), 1367–1375. https://doi.org/10.1007/BF03177422

Lam, G. C. Y., & Leung, R. C. K. (2018). Aeroacoustics of NACA 0018 airfoil with a cavity. *AIAA Journal*, *56*(12), 4775–4786. https://doi.org/10.2514/1.J056389

Liu, T., Montefort, J., Liou, W., & Pantula, S. (2010). Effects of flexible fin on low-frequency oscillation in post-stall flows. *AIAA Journal*, *48*(6), 1235–1247. https://doi.org/10.2514/1.J050205

McMasters, J. H., & Henderson, M. L. (1979). Low speed single-element airfoil synthesis. *Technical Soaring*, *6*(2), 1–21.

Meyer, R., Hage, W., Bechert, D. W., Schatz, M., Knacke, T., & Thiele, F. (2007). Separation control by self-activated movable flaps. *AIAA Journal*, *45*(1), 191–199. https://doi.org/10.2514/1.23507

Mizoguchi, M., & Itoh, H. (2013). Effect of aspect ratio on aerodynamic characteristics at low Reynolds numbers. *AIAA Journal*, *51*(7), 1631–1639. https://doi.org/10.2514/1.J051915

Moffat, R. J. (1988). Describing the uncertainties in experimental results. *Experimental Thermal and Fluid Science*, *1*, 3–17. https://doi.org/10.1016/0894-1777(88)90043-X

Mueller, T. J. (1999). *Aerodynamic measurements at low Reynolds numbers for fixed wing micro-air vehicles*. RTO AVT/VKI Special Course on Development and Operation of UAVs for Military and Civil Applications, University of Notre Dame.

Mueller, T. J., Kellogg, J. C., Ifju, P. G., & Shkarayev, S. V. (2007). *Introduction to the Design of Fixed-Wing Micro Air Vehicles: Including Three Case Studies*. American Institute of Aeronautics and Astronautics. https://doi.org/10.2514/4.862106

Nelson, R. C. (1998). *Flight stability and automatic control*. 2nd Edition, Mc Graw Hill, New York.

Okamoto, M., & Azuma, A. (2011). Aerodynamic characteristics at low Reynolds numbers for wings of various planforms. *AIAA Journal*, *49*(6), 1135–1150. https://doi.org/10.2514/1.J050071

Park, D., Shim, H., & Lee, Y. (2020). PIV Measurement of separation bubble on an airfoil at low Reynolds numbers. *Journal of Aerospace Engineering*, *33*(1), 04019105: 1-17. https://doi.org/10.1061/(asce)as.1943-5525.0001099

Pelletier, A., & Mueller, T. J. (2000). Low Reynolds number aerodynamics of low-aspect-ratio, thin/flat/cambered-plate wings. *Jornal of Aircraft*, *37*(5), 825–832. https://doi.org/10.2514/2.2676

Rizzetta, D. P., & Visbal, M. R. (2008). Plasma-based flow-control strategies for transitional highly loaded low-pressure turbines. *Journal of Fluids Engineering, Transactions of the ASME*, *130*(4), 0411041–04110412. https://doi.org/10.1115/1.2903816

Rizzetta, D. P., & Visbal, M. R. (2012). Plasma control for a maneuvering low-aspect-ratio wing at low reynolds number. *Journal of Fluids Engineering, Transactions of the ASME*, *134*(12), 1–19. https://doi.org/10.1115/1.4007947

Schatz, M., Knacke, T., Thiele, F., Meyer, R., Hage, W., & Bechert, D. (2004, January 5-8). *Separation control by self-activated movable flaps*. 42nd AIAA Aerospace Sciences Meeting and Exhibit, Reno, Nevada. https://doi.org/10.2514/6.2004-1243

Schlüter, J. U. (2010). Lift enhancement at low Reynolds numbers using self-activated movable flaps. *Journal of Aircraft*, *47*(1), 348–351. https://doi.org/10.2514/1.46425

Selig, M. S., Lyon, C. A., Giguere, P., Ninham, C. P., & Guglielmo, J. J. (1996). *Summary of Low-Speed Airfoil Data*, Vol 2. SoarTech Publications, Virginia Beach.

Verma, A., & Kulkarni, V. (2021, November 1-5). *Effect of self-actuating flap on the aerodynamic performance of flat plate wing at low Reynolds number*. ASME International Mechanical Engineering Congress and Exposition. https://doi.org/10.1115/IMECE2021-70495

Wang, C. H. J., & Schlüter, J. (2012). Stall control with feathers: Self-activated flaps on finite wings at low Reynolds numbers. *Comptes Rendus - Mecanique*, *340*(1–2), 57–66. https://doi.org/10.1016/j.crme.2011.11.001

Winslow, J., Otsuka, H., Govindarajan, B., & Chopra, I. (2018). Basic understanding of airfoil characteristics at low Reynolds numbers (10^4–10^5). *Journal of Aircraft*, *55*(3), 1050–1061. https://doi.org/10.2514/1.C034415